ORIGINAL ARTICLE

Empirical formula model and process parameter optimization of two-dimensional ultrasonic-assisted grinding force based on 2.5D-Cf/SiC fiber orientation

Yashuai Wang[1] · Bo Xin[1] · Jiangtao Li[2] · Lida Zhu[1]

Abstract

Due to the anisotropic characteristic of carbon fiber-reinforced silicon carbide ceramics, the fiber orientation angle significantly affects the grinding force. Therefore, it is important to study the influence rule of different fiber orientations on the grinding force of 2.5D-C_f/SiC composites. To study the comprehensive influence of machine tool parameters and the anisotropy of carbon fiber-reinforced ceramic matrix composites on the grinding force, two-dimensional ultrasonic plane grinding was studied by orthogonal test and single-factor experiment. Based on the multi-exponential fitting analysis method of multiple linear regression equation, the empirical equations of power exponential grinding force prediction model of 2D ultrasonic-assisted grinding and conventional grinding 2.5D-C_f/SiC composites at 0°, 45°, and 90° fiber orientation and considering fiber orientation and ultrasonic amplitude were established, respectively. To verify the empirical formula model in predicting the grinding force of 2.5D-C_f/SiC composites under various fiber orientation angles, the regression equation and regression coefficient of the model were examined. The influence of 2.5D-C_f/SiC grinding parameters on the grinding force was analyzed. The parameters of the grinding force model were optimized based on range analysis and variance analysis, and the optimal process parameter combination was obtained. The results show that the grinding force is negatively correlated with the linear speed and positively correlated with the feed speed and grinding depth within the range of experimental parameters. The maximum reduction of the normal grinding force is 29.78% when the line speed is 10.48 m/s, the feed speed is 100 mm/min, the grinding depth is 50 μm, and along the 45° fiber direction. The optimal grinding parameter combination is a line speed of 23.60 m/s, feed speed of 5 mm/min, and grinding depth of 10 μm along the 0° fiber orientation.

Keywords 2.5D-C_f/SiC composites · Fiber orientation · Parameter optimization · Two-dimensional ultrasound · Empirical equation

1 Introduction

2.5D-C_f/SiC is a composite material with silicon carbide ceramics as the matrix and high-toughness carbon fiber as the reinforcement phase [1]. The needled fiber in the Z direction penetrates the continuous carbon fiber layer in the X and Y directions [2], so that 2.5D-C_f/SiC has higher toughness and strength than 1D-C_f/SiC and 2D-C_f/SiC [3]. 2.5D-C_f/SiC in addition to the advantages of silicon carbide such as high hardness, high-temperature resistance, corrosion resistance, wear resistance, low density, and ease of adapting to extreme environments [4] also greatly compensates for its disadvantages such as high brittleness [5]. 2.5D-C_f/SiC composites are currently recognized as one of the advanced high-temperature structural ceramic materials and friction and wear materials [6], which are mainly used in the field of aerospace and automotive brake systems [7]. 2.5D-C_f/SiC composites are commonly used in the machining of high-temperature-resistant structural components such as thermal shielding layers on spacecraft and nozzle-guided blades on aero-engines [8], to be adapted to extremely high temperatures and high pressures in the operating environment [9]. 2.5D-C_f/SiC composites with high temperature and wear resistance [10] are often used in the field of automotive brake discs to provide better braking performance [11]. Due to the high hardness and high brittleness of 2.5D-C_f/SiC, severe machined surface damage and tool wear can easily occur during conventional machining [12]. Ultrasonic-assisted grinding is an assisted machining method that applies ultrasonic vibration to the grinding process [13]. Especially for the

✉ Bo Xin
xinbo@me.neu.edu.cn

1 School of Mechanical Engineering and Automation, Northeastern University, Shenyang 110819, Liaoning, China

2 Gongyi Fanrui Yihui Composite Material Co, Zhengzhou 451261, Henan, China

machining of hard and brittle materials, ultrasonic vibration achieves better machining performance by changing the contact state between the abrasive particles and the workpiece [14]. Studies have shown that ultrasound-assisted grinding of 2.5D-C_f/SiC can reduce the grinding force and improve the surface quality more effectively than conventional grinding [15]. The anisotropy and inhomogeneity of 2.5D-C_f/SiC composites [16, 17] have led to the fact that aspects of the material removal mechanism and mathematical modeling of ultrasound-assisted grinding remain poorly understood.

Based on the many advantages of 2.5D-C_f/SiC composites, in recent years, more and more scholars have tended to study the processing mechanism of grinding C/SiC composites. Kun Zhou et al. [18–20] investigated the removal mechanism of C_f/SiC composites by laser ablation-assisted single-grain scratch grinding as well as belt grinding experiments, which showed that the grinding force, grinding temperature, surface roughness, and diamond wear of C_f/SiC composites were significantly reduced during laser ablation-assisted grinding. The main manifestations were microfracture and toughness removal, which enhanced the plastic domain removal behavior of the material. Jie Chen et al. [21–23] conducted ultrasound-assisted milling laser ablation experiments on C_f/SiC composites to investigate the microfracture mechanism and transformation mechanism of carbon fibers, and the results showed that ultrasonic vibration could reduce the milling temperature and milling force. Ultrasound-assisted milling promotes the removal of carbon fibers from nanoscale brittle fractures by reducing the maximum undeformed chip thickness, thus improving the machined surface quality. Zhigang Dong et al. [24, 25] developed a grinding force model for ultrasound-assisted grinding of ceramic matrix composites from the perspective of anisotropy and inhomogeneity so that the ultrasound-assisted grinding force can be well predicted. Guoyan Sun et al. [26] modeled three grinding force components, namely the plastic removal stage, brittle removal stage, and friction stage, in the ultrasonic grinding process by studying the thickness of undeformed cutting chips. The results showed that axial ultrasonic vibration could reduce the surface roughness by 18.0% and the normal and tangential forces by 27.31% and 22.52%, respectively. Yi-Feng Xiong et al. [27] investigated ultrasonic-assisted grinding of SiC/SiC composites, and the results showed that ultrasonic vibration-assisted machining technology is a suitable machining method for this material under suitable tool conditions. Xingzhi Xiao et al. [28] established a theoretical model of cutting force from the perspective of ultrasonically assisted grinding of zirconia ceramics with tough and brittle transition removal mechanism, which can well predict the critical grinding depth of tough removal and brittle removal transitions, to better understand the effect of tough fracture and brittle fracture mechanisms on the grinding force. Xiaofei Lei et al. [29] conducted ultrasound-assisted single-grain high-speed grinding experiments from different abrasive wear aspects. A novel dynamic grinding force model

for ultrasound-assisted high-speed grinding of single-grain abrasives was established. Wei Li et al. [30] investigated the material removal mechanism of laser-assisted grinding of 3D-C_f/SiC from the perspective of the effect of laser parameters on material damage and came up with the results that laser heating can reduce the hardness of the material, achieving the removal of toughness region, and reduce the grinding force to improve the surface quality. At present, most experts study the grinding processing of C_f/SiC composites mainly focusing on process and experimental studies. Due to the anisotropic and inhomogeneous characteristics of C_f/SiC composites, the mechanism of the grinding force in its grinding process has not been understood thoroughly. Currently, the theoretical models for 2D ultrasound-assisted 2.5D-C_f/SiC are still not well researched; therefore, this study explores in depth the grinding force model for 2D ultrasound-assisted grinding of 2.5D-C_f/SiC. A few scholars have done a small amount of research on analytical and numerical theoretical models for grinding 2.5D-C_f/SiC. Still, the studies done are not sufficient to provide an in-depth explanation of the grinding forces in two-dimensional ultrasound-assisted grinding (TDUAG) and machining of 2.5D-C_f/SiC taking into account the fiber orientation of the material and the ultrasound amplitude. Based on the influence of ultrasonic amplitude, fiber orientation, process parameters, and other factors on the grinding force of 2.5D-C_f/SiC processed by TDUAG, an empirical formula model of the grinding force of TDUAG of 2.5D-C_f/SiC was constructed. This study is an important reference value for operators in engineering practice to control the grinding force to optimize the machining accuracy in precision machining of C_f/SiC composites.
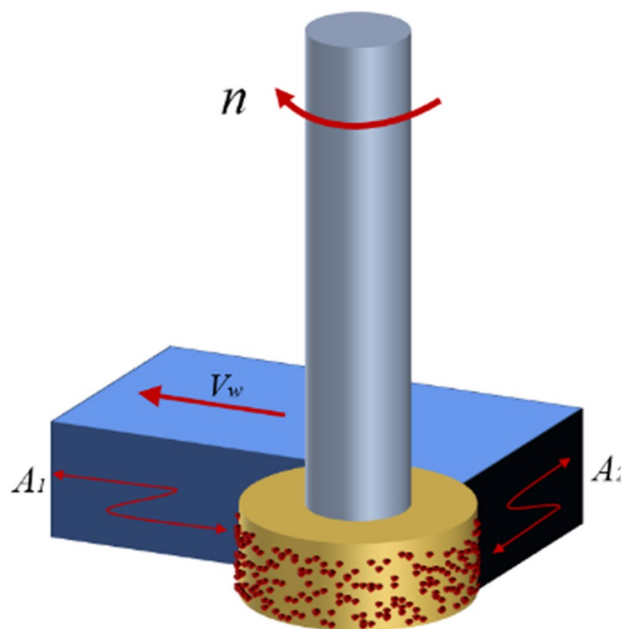

Fig. 1 Motion diagram of 2D ultrasonic-assisted grinding

2 Mechanism analysis of TDUAG and experimental conditions

2.1 Kinematic analysis of single grit for TDUAG

The principle of two-dimensional ultrasonic-assisted grinding is to change the relative motion trajectory of the abrasive grain and the workpiece by applying an elliptical ultrasonic vibration signal, to realize a series of excellent grinding processing characteristics. The motion of 2D ultrasonic-assisted grinding is shown in Fig. 1, including the rotary motion of the spindle, the linear feed motion, and the ultrasonic motion superimposed on the X and Y directions. Figure 2 shows a schematic diagram of the motion trajectory of a single grit for conventional grinding (CG) and TDUAG, and the motion trajectory equations and velocity equations of a single grit for conventional grinding and TDUAG can be expressed as the following Eqs. (1) and (2), respectively:

$$S_{TDUAG}(t) = \left[\begin{array}{l} S_{xTDUAG}(t) = R \cdot (1 - cos\phi) + A_1 \cdot cos(\omega_1 t + \phi_1) = R - R \cdot cos\phi + A_1 \cdot sin\omega_1 t \\ S_{yTDUAG}(t) = V_w \cdot t + R \cdot sin\phi + A_2 \cdot cos(\omega_2 t + \phi_2) = V_w \cdot t + R \cdot sin\phi + A_2 \cdot sin\omega_2 t \end{array} \right] \quad (1)$$

$$V_{TDUAG} = \left[\begin{array}{l} V_{xTDUAG}(t) = \frac{dS_{xTDUAG}(t)}{dt} = R \cdot \omega \cdot sin\omega t + A_1 \cdot \omega_1 \cdot cos\omega_1 t \\ V_{yTDUAG}(t) = \frac{dS_{yTDUAG}(t)}{dt} = V_w + R \cdot \omega \cdot cos\omega t + A_2 \cdot \omega_2 \cdot cos\omega_2 t \end{array} \right] \quad (2)$$

The equations of trajectory and velocity of a single diamond grit for routinely grinding 2.5D-C/SiC composites can be expressed as shown in Eqs. (3) and (4), respectively:

$$S_{CG}(t) = \left[\begin{array}{l} S_{xCG}(t) = R - R \cdot cos\phi = R \cdot (1 - cos\omega t) \\ S_{yCG}(t) = S_w(t) + R \cdot sin\phi = V_w \cdot t + R \cdot sin\omega t \end{array} \right] \quad (3)$$

$$V_{CG}(t) = \left[\begin{array}{l} V_{xCG}(t) = \frac{dS_{xCG}(t)}{dt} = R \cdot \omega \cdot sin\omega t \\ V_{yCG}(t) = \frac{dS_{yCG}(t)}{dt} = V_w + R \cdot \omega \cdot cos\omega t \end{array} \right] \quad (4)$$

From the kinematic trajectory equations and velocity equations of a single grit, it can be deduced that the contact arc length of a single grit for 2D ultrasound-assisted grinding and conventional grinding is:

where $S_{TDUAG}(t)$, $V_{TDUAG}(t)$ and $S_{CG}(t)$, $V_{CG}(t)$ are the trajectories and speeds of a single grit of TDUAG and CG, respectively, in time t. R is the diameter of the grinding wheel, $Sw(t)$ is the feed motion of the workpiece, V_w is the feed speed of the workpiece, t is the time of the rotation of a single grit, ϕ is the angle of a single grit turning in time t, and is the angular speed of a single grit turning. The angular velocity of the rotation of a single grit. A_1 and A_2 are the ultrasound amplitudes of the 2D ultrasound platform, respectively. $A1 = A2 = 6~\mu m$. ϕ_1, ϕ_2 $\omega_1 = \omega_2 = 2\pi \cdot f_1 = 2\pi \cdot f_2$, $f_1 = f_2 = 20000 Hz$, are the phase angles of the two-dimensional ultrasonic vibration platform, respectively. $\phi_1 = \phi_2 = 90°$. l_{TDUG}, l_{CG} are the contact arc lengths of single grits for TDUAG and CG, respectively.

$$l_{TDUAG} = \sqrt{V_x(t)^2 + V_y(t)^2} = \sqrt{(R \cdot \omega \cdot sin\omega t + A_1 \cdot \omega_1 \cdot cos\omega_1 t)^2 + (V_w + R \cdot \omega \cdot cos\omega t + A_2 \cdot \omega_2 \cdot cos\omega_2 t)^2} dt$$

$$l_{CG} = \sqrt{V_{xCG}(t)^2 + V_{yCG}(t)^2} = \sqrt{(R \cdot \omega \cdot sin\omega t)^2 + (V_w + R \cdot \omega \cdot cos\omega t)^2} dt \quad (5)$$

Fig. 2 Motion path diagram of two-dimensional ultrasonic-assisted single grit grinding
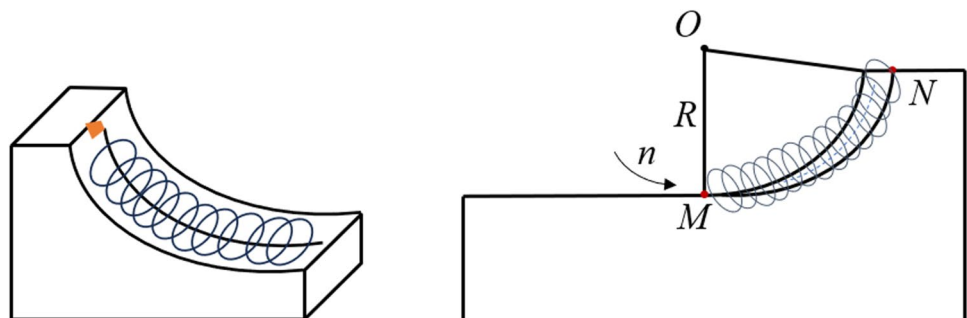
From the comparison of the two equations in Eq. (5), it can be seen that l_{TDUG} is longer than l_{CG}, and the difference between them is caused by the amplitude and frequency of ultrasonic vibration. The application of 2D ultrasound increases the contact arc length between the abrasive grain and the workpiece. According to the literature [31], the average cross-sectional area of chips $a_{g\max}$ can be expressed by formula (6):

$$a_{g\max} = [\frac{v_w}{v_s} \cdot a_p] \cdot [\frac{2}{N_{dl} \cdot l_s}] \tag{6}$$

Therefore, the average cross-sectional area of chips $a_{g\max}$ is inversely proportional to the contact arc length. Therefore, the average cross-sectional area of chips $a_{g\max}$ will be reduced when 2D ultrasonic-assisted grinding of a single abrasive particle is applied. By referring to the literature [31], we can see that the average cross-sectional area of chips $a_{g\max}$ can also be expressed by the formula (7):

$$a_{g\max} = \frac{1}{A_{g1}^p}[\frac{2}{c_1 k_s}]^{\frac{1}{p+1}}[\frac{v_w}{v_s}]^{\frac{1}{p+1}}[\frac{a_p}{d_e}]^{\frac{1}{2(p+1)}} \tag{7}$$

Therefore, the average chip cross-sectional area $a_{g\max}$ is proportional to the grinding depth a_p. As a result, the average cross-sectional area of chips $a_{g\max}$ is reduced when 2D ultrasonic-assisted grinding is applied to a single particle. It is also known from relevant literature [31] that the formula of normal grinding force F_n and tangential grinding force F_t per unit grinding width can be expressed by formula (8) and formula (9), respectively:

$$F_n = K\frac{v_w}{v_s} \cdot a_p + \frac{A_g \overline{\delta p}}{1+\alpha}[c_1]^{\beta}[\frac{v_w}{v_s}]^{\alpha}[a_p]^{\frac{1+\alpha}{2}}[d_e]^{\frac{1-\alpha}{2}} \tag{8}$$

$$F_t = \varphi K\frac{v_w}{v_s}a_p + \frac{A_g \mu \overline{\delta p}}{1+\alpha}[c_1]^{\beta}[\frac{v_w}{v_s}][a_p]^{\frac{1+\alpha}{2}}[d_e]^{\frac{1-\alpha}{2}} \tag{9}$$

According to formulas (8) and (9), the normal grinding force and tangential grinding force per unit grinding width are proportional to the grinding depth a_p. Therefore,

applying 2D ultrasonic-assisted grinding can reduce grinding force.

2.2 Workpiece material

The workpiece material is a 2.5D-C_f/SiC composite fabricated by reactive melt infiltration (RMI). Its microstructure is shown in Fig. 3. The specific components include continuous carbon fiber layup in the X direction with constant carbon fiber layup in the Y direction (T700, carbon fiber volume fraction of $\varphi_c = 50\%$, orthogonal layup of carbon fiber bundles), needled fibers in Z direction, SiC matrix, and a small number of pores with 10% porosity. The workpiece size is $7 \times 7 \times 4$ mm, and Table 1 shows the mechanical property parameters of 2.5D-C_f/SiC composites. The schematic structure of the 2.5D-C_f/SiC composite is shown in Fig. 4.

2.3 Experimental instruments and schemes

The grinding experiments were carried out on a TCR500 vertical machining center shown in Fig. 5. Table 2 shows the main technical parameters of the machine. Table 3 shows the technical parameters of the grinding wheel. The 2D ultrasonic-assisted grinding platform is a 2D ultrasonic vibrating platform integrated into the machining center table, as shown in Fig. 6. The ultrasonic amplitude is changed by controlling the power percentage and phase angle of the ultrasonic device in X and Y directions through the ultrasonic generator. Figure 6 shows the three-dimensional structure of the two-dimensional ultrasonic vibration platform, and the two-dimensional ultrasonic vibration platform is composed of a set of amplitude-variable rods and transducers in the X

Table 1 2.5D-C_f/SiC material parameter performance

Material parameters	Value
Tensile strength (MPa)	100–150
Curved strength (MPa)	160–270
Compress strength (MPa)	280–310
Volume density (g/cm³)	2.0

Fig. 3 2.5D-C_f/SiC microstructure diagram

Y- Carbon fiber bundle
X- Carbon fiber bundle
Z-Needle-punched fibers
SiC matrix
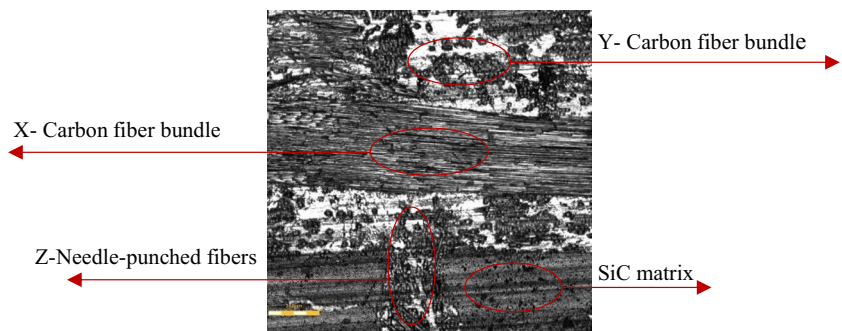
Fig. 4 2.5D-C_f/SiC three-dimensional structure diagram
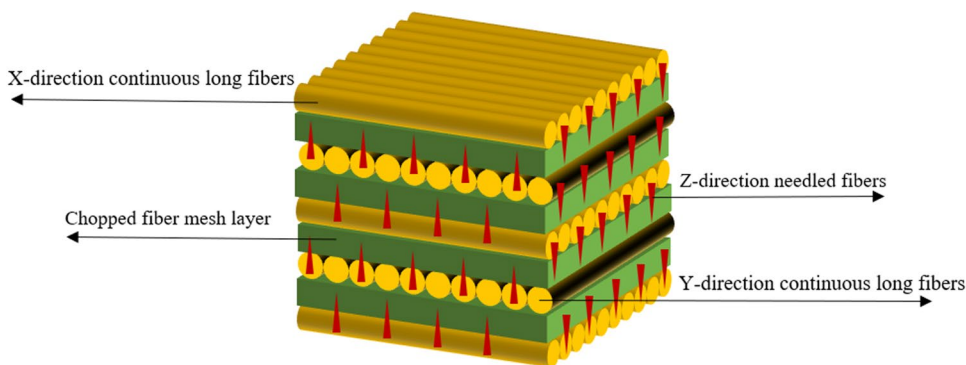
Fig. 5 TCR500 vertical machining center

Table 2 Technical parameters of the machine

Technical parameters	Value
Maximum spindle speed (r/min)	20000
Machine table size (mm)	650×400
Positioning accuracy of X, Y, and Z axes (mm)	0.01
Maximum travel of X, Y, and Z axes (mm)	$500 \times 400 \times 300$

Table 3 Technical parameters of the grinding wheel

Technical parameters	Value
Grinding wheel type	Electroplated diamond wheel
Grinding wheel diameter (mm)	25
Grinding wheel size (#)	150
Shank diameter (mm)	10

the 20,000 Hz ultrasonic generator together. Figure 7 shows the two-dimensional ultrasonic-assisted grinding processing platform.

A Kistler 9119AA2 six-degree-of-freedom force gauge captured the grinding force. The working principle is that the piezoelectric crystal sensor collects the signal of grinding force and then transmits it in the form of a voltage signal to the 5080 charge amplifier for amplification. After, the amplified voltage signal is transmitted to the 5697 data acquisition card in the first A/D conversion, that is, the voltage signal is converted to a binary form of digital signals; the next step in the D/A conversion, that is, the binary digital signal, is converted to a decimal analog signal. Finally, the data acquisition card will be converted to voltage signal transmission to the host PC DynoWare software output grinding force. In the experiment, the force measuring instrument that collects the grinding force may generate a slight vibration signal. To ensure the accuracy of the collected ultrasonic-assisted grinding force, all the grinding force signals in this study were zero drift compensated and filtered, and then the net grinding force value was obtained by subtracting the vibration interference signal of the dynamometer from the total collected grinding force.

The main process parameters affecting the 2.5D-C_f/SiC grinding force are the grinding wheel line speed, workpiece feed speed, grinding depth, and C_f/SiC fiber orientation. Therefore, the orthogonal test method of three factors and four levels was adopted, and the orthogonal table of L16
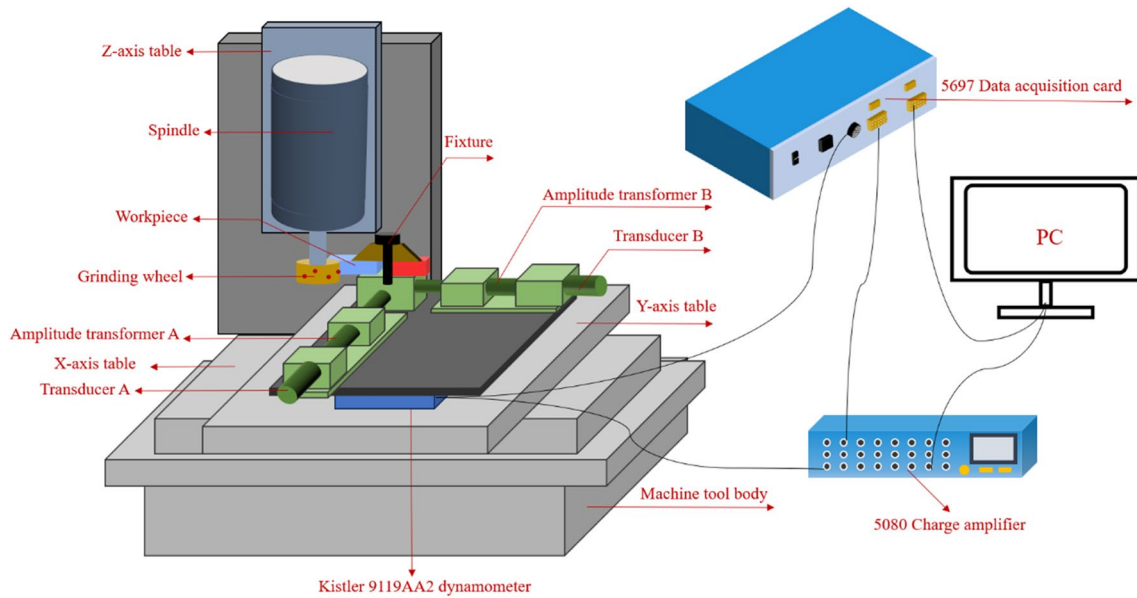
direction and a set of amplitude-variable rods and transducers in the Y direction, as well as a porous universal platform connecting the ultrasound in the X and Y directions, and

Fig. 6 Schematic diagram of 2D ultrasonic-assisted grinding processing platform

Fig. 7 Two-dimensional ultrasonic-assisted grinding platform [32]
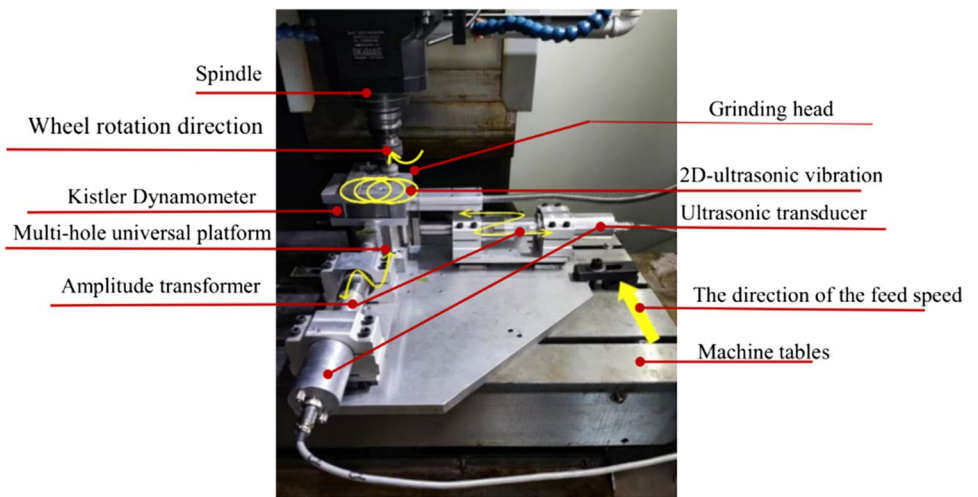
(43) was selected. Table 4 is a horizontal table of process parameter factors for grinding 2.5D-C_f/SiC.

3 Results and discussion

3.1 Influence of process parameters on grinding force

As shown in Table 4, the effects of wheel speed, feed rate, and grinding depth on the grinding force when CG and TDUAG of 2.5D-C_f/SiC composites along the three fiber orientations of 0°, 90°, and 45° are shown in Fig. 8a–c, Fig. 8d–f, and Fig. 8g–i, respectively,

Table 4 Processing test parameters

Level	Factor		
	Linear speed v_s/ (m/s)	Feed speed v_w/(mm/ min)	Grinding depth a_p/ (N)
	A	*B*	*C*
1	0.66	5	10
2	2.36	20	50
3	10.48	50	100
4	23.6	100	150

while keeping the feed rate of 50 mm/min and the depth of grinding at 50 µm. It can be seen that in the range of parameters of this experiment, with or without the application of ultrasound, the normal grinding force and tangential grinding force decrease with the increase of the linear speed of the grinding wheel, with the increase of the linear speed *Vs*, the number of abrasive grains acting on the surface of the grinding process per unit of time increases, and the thickness of the chip of a single abrasive grain becomes smaller, and the grinding force decreases. The grinding force increases with the increase of feed speed and grinding depth. With the increase of grinding depth ap and table feed speed, the number of effective abrasive grains

increases, the relative contact area between abrasive grains and workpiece increases, the total amount of material removed per unit of time increases, and the thickness of the chip of abrasive grains becomes larger, which increases the grinding force. Under the same machining parameters, the grinding force after applying TDUAG was significantly smaller than the CG force, which was because the contact arc length of a single grit with ultrasonic-assisted grinding was larger than that without ultrasonic, and the maximum undeformed chip thickness of material removed by the grits per unit of time was inversely proportional to the contact arc length, and therefore, the maximum undeformed chip thickness of a single grit was reduced by
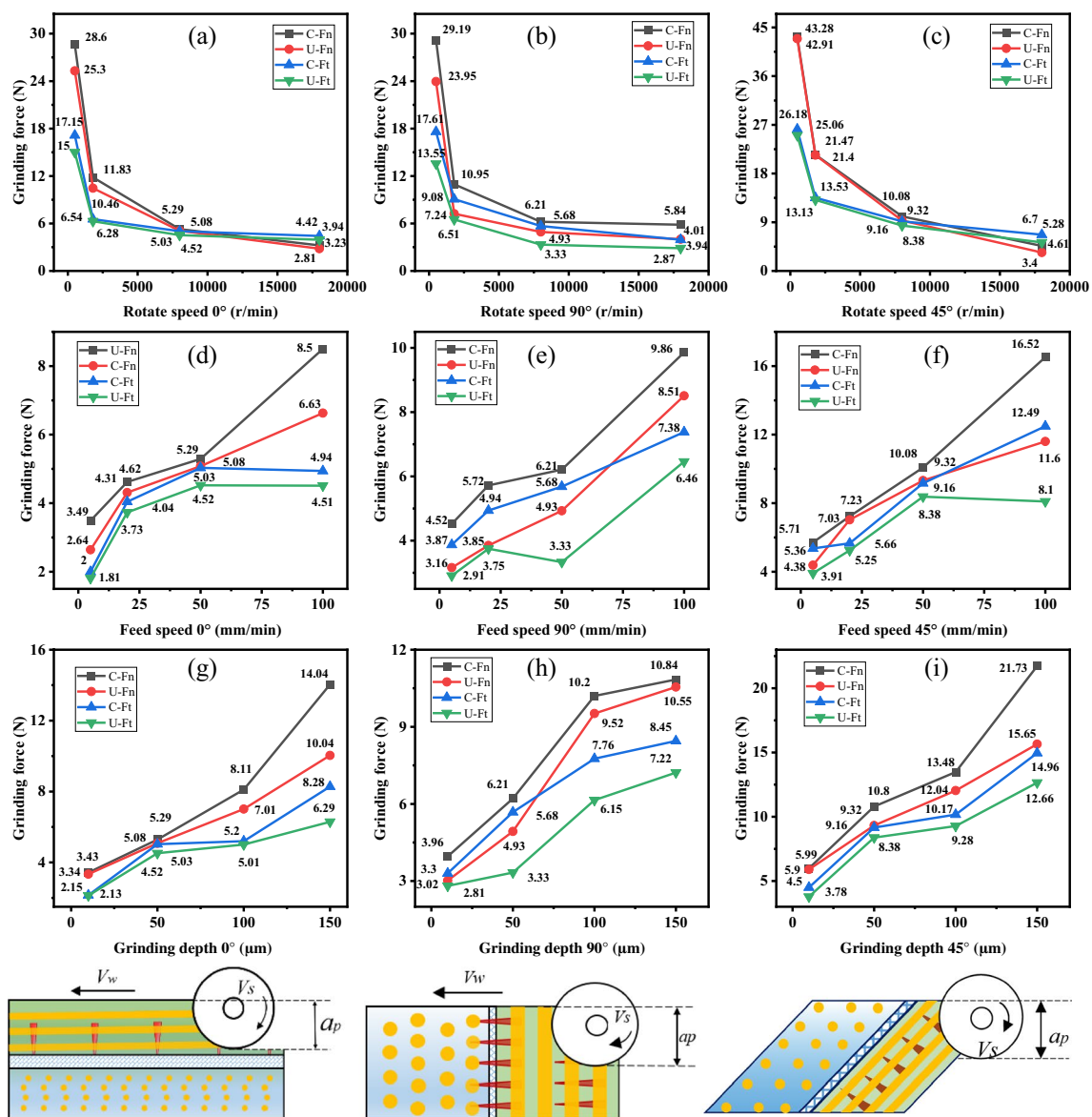

Fig. 8 Influence of process parameters on grinding force

applying ultrasonic vibration. The grinding force of the grits was proportional to the maximum undeformed chip thickness, so the grinding force assisted by the application of 2D ultrasonic vibration was reduced compared with the normal grinding force. The maximum percentage reduction in normal grinding force was 29.78% for grinding along the 45° fiber orientation with a feed rate of 100 mm/min. Due to the anisotropy and inhomogeneity between the reinforcing fiber phase of 2.5D-C_f/SiC composites and the silicon carbide ceramic matrix, the variation of the grinding force concerning the process parameters is not linear.

The surface morphology of ground 2.5D-C_f/SiC with fiber orientations taken at 0°, 45°, and 90° are shown in Fig. 9a, b, and c, respectively. As shown in Fig. 9a, when grinding along the 0° fiber orientation, the fiber is compressed and deformed, followed by fiber stripping, and finally fiber wear until the fiber breaks to form a new surface. As shown in Fig. 9b, when grinding along the 90° fiber orientation, the fiber shear deformation occurs, followed by fiber stripping, and finally fiber wear until the fiber breaks to form a new surface. As shown in Fig. 9c, when grinding along the 45° fiber orientation, the fiber has both extrusion deformation and shear deformation and finally fiber wear. From Fig. 9, it can be found that the three fiber orientations fracture in different ways. Therefore, it is of great importance to study the effect of fiber orientation on the grinding process. It is very necessary to establish an empirical formula model considering the effect of fiber orientation on the grinding force.

3.2 Orthogonal experimental design results

Table 5 shows the orthogonal test table of three factors and four levels of the influence of process parameters such as line speed, feed speed, and grinding depth on the grinding force of 2.5D-C_f/SiC, and the test results.

3.3 5D-C_f/SiC empirical equation model of grinding force

3.3.1 Empirical formula model for grinding forces in different *fiber* directions

2.5D-C_f/SiC composites have a very complex structural arrangement due to the different properties of the reinforcing phase carbon fibers and the SiC matrix material, as well as the material's internal structure. Therefore, C_f/SiC has obvious anisotropy and inhomogeneity. The inhomogeneity and anisotropy of C_f/SiC lead to a different material removal mechanism during the grinding process than that of SiC materials. Its grinding material removal mechanism is still unclear. At present, there is still no very accurate predictive model relationship equation between grinding process parameters such as grinding wheel linear speed, feed rate, grinding depth, and grinding force. Based on this research gap, the specific relationship between grinding process parameters and grinding force was investigated. An empirical formula prediction model for the grinding force of 2.5D-C_f/SiC composites was established.

Model the empirical equation of the power exponential form of the grinding force, set Eq. (10):

$$F = \lambda \cdot v_s^{\alpha} \cdot v_w^{\beta} \cdot a_p^{\gamma} \tag{10}$$

where λ is the empirical coefficient and α, β, γ, are the coefficient to be determined concerning the modeled process parameters.

To facilitate the calculation of the equality coefficients, Eq. (11) is obtained by taking logarithms on both sides of the equality sign:

$$\lg F = \lg \lambda + \alpha \cdot \lg v_s + \beta \cdot \lg v_w + \gamma \cdot \lg a_p \tag{11}$$

Make

$$Y = \lg F, X_0 = \lg \lambda, X_1 = \lg v_s, X_2 = \lg v_w, X_3 = \lg a_p$$
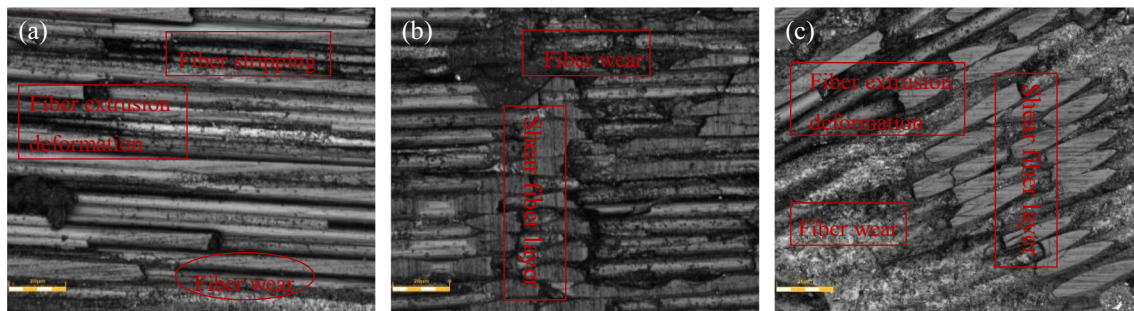
Then Eq. (12) can be converted to

Fig. 9 Three fiber-oriented grinding surface morphology

Table 5 Table of orthogonal test results of 2.5D-C/SiC grinding force

Test number	Element association			Test results											
M	v_s (m/s)	v_w (mm/min)	a_p (μm)	0°	45°	90°	0°	45°	90°	0°	45°	90°	0°	45°	90°
				U-F_n/(N)			C-F_n/(N)			U-F_t/(N)			C-F_t/(N)		
1	0.66	5	10	1.04	1.77	1.46	1.57	3.46	1.86	0.102	1.55	0.37	0.549	1.17	0.59
2	0.66	20	50	16.118	19.6	17.35	17.753	19.9	22.19	9.284	10.85	10.42	10.97	11.67	13.45
3	0.66	50	100	42.24	37.65	4 9.11	49.96	45.65	59.8	27.83	24.54	29.05	32.68	28.67	35.61
4	0.66	100	150	49.6	42.26	73.84	95.70	82.64	109.80	32.86	27.47	44.16	64.01	49.83	65.53
5	2.36	5	50	4.13	6.37	2.92	5.07	7.64	3.83	0.87	1.83	1.07	1.87	2.68	1.96
6	2.36	20	10	2.05	3.04	2.46	2.54	5.11	3.05	0.24	1.88	1.27	0.86	2.61	1.56
7	2.36	50	150	34.9	37.46	34.8	39.17	44.16	36.21	23.53	25.35	21.64	26.12	30.61	23.88
8	2.36	100	100	38.8	37.45	27.06	41.76	42.42	36.99	25.13	22.79	16.55	27.29	28.54	22.39
9	10.56	5	100	1.92	2.29	0.93	2.53	3.50	1.52	0.26	2.43	0.57	1.48	2.64	0.98
10	10.56	20	150	7.93	2.10	6.19	10.32	7.38	7.66	4.92	1.48	3.78	6.50	4.38	4.76
11	10.56	50	10	1.05	0.88	0.94	1.44	2.08	1.57	0.23	0.32	0.57	0.72	1.26	0.88
12	10.56	100	50	9.73	12.24	12.27	11.53	13.51	13.03	5.35	5.61	6.53	6.44	7.61	7.24
13	23.6	5	150	1.23	2.55	0.85	1.98	3.16	1.64	0.19	1.30	0.49	0.85	1.62	0.96
14	23.6	20	100	5.17	8.51	2.20	5.49	10.18	2.86	1.59	3.05	1.49	3.10	5.26	1.64
15	23.6	50	50	4.07	3.94	3.12	4.34	4.79	4.65	1.56	2.12	1.92	2.22	2.51	2.51
16	23.6	100	10	0.41	1.83	1.00	1.22	2.53	1.60	0.31	0.88	0.48	0.58	1.41	0.75

$$Y = X_0 + \alpha \cdot X_1 + \beta \cdot X_2 + \gamma \cdot X_3 \tag{12}$$

Based on the multiple linear regression equation, the transformed experimental data were regressed and analyzed to find the values of the coefficients in Eq. (12).

$$X_0, \alpha, \beta, \gamma$$

The value in Eq. (11) is then inverted. An empirical formula prediction model for grinding force in power exponential form can be derived. Based on the experimental results, the following empirical formula is established with the grinding force as the target:

The normal and tangential grinding forces for CG were modeled for fiber orientations of 0°, 45°, and 90° in Eq. (13), (14), respectively:

$$\begin{cases} 0° : F_n = 10^{-1.129} \cdot v_s^{-0.5531} \cdot v_w^{0.5985} \cdot a_p^{0.8719} \\ 45° : F_n = 10^{-0.513} \cdot v_s^{-0.5006} \cdot v_w^{0.4829} \cdot a_p^{0.6586} \\ 90° : F_n = 10^{-1.014} \cdot v_s^{-0.6365} \cdot v_w^{0.7085} \cdot a_p^{0.7346} \end{cases} \tag{13}$$

$$\begin{cases} 0° : F_t = 10^{-2.728} \cdot v_s^{-1.000} \cdot v_w^{1.165} \cdot a_p^{1.447} \\ 45° : F_t = 10^{-1.065} \cdot v_s^{-0.481} \cdot v_w^{0.5749} \cdot a_p^{0.7459} \\ 90° : F_t = 10^{-1.542} \cdot v_s^{-0.616} \cdot v_w^{0.7492} \cdot a_p^{0.8504} \end{cases} \tag{14}$$

The normal and tangential grinding force models for TDUAG at fiber orientations of 0°, 45°, and 90°, respectively, are as follows in Eq. (15), (16):

$$\begin{cases} 0° : F_n = 10^{-1.341} \cdot v_s^{-0.5789} \cdot v_w^{0.5697} \cdot a_p^{0.956} \\ 45° : F_n = 10^{-0.806} \cdot v_s^{-0.0508} \cdot v_w^{0.51} \cdot a_p^{0.713} \\ 90° : F_n = 10^{-1.189} \cdot v_s^{-0.6861} \cdot v_w^{0.7422} \cdot a_p^{0.7483} \end{cases} \tag{15}$$

$$\begin{cases} 0° : F_t = 10^{-2.938} \cdot v_s^{-0.6195} \cdot v_w^{1.058} \cdot a_p^{1.225} \\ 45° : F_t = 10^{-1.846} \cdot v_s^{-0.627} \cdot v_w^{0.8367} \cdot a_p^{0.8747} \\ 90° : F_t = 10^{-1.047} \cdot v_s^{-0.5821} \cdot v_w^{0.473} \cdot a_p^{0.764} \end{cases} \tag{16}$$

3.3.2 Empirical formulation model of grinding force considering 2D ultrasound and *fiber* orientation angle

Model the empirical equation of the power exponential form of the grinding force, set Eq. (17):

$$F = \varepsilon \cdot v_s^a \cdot v_w^b \cdot a_p^c \cdot \theta^d \tag{17}$$

In Eq. (17) ε is the empirical coefficient and a, b, c, d are the coefficients to be determined concerning the model process parameters and fiber orientation angle.

To facilitate the calculation of the coefficients of equivalence, Eq. (18) is obtained by taking logarithms on both sides of the equal sign:

$$\lg F = \lg \varepsilon + a \cdot \lg v_s + b \cdot \lg v_w + c \cdot \lg a_p + d \cdot \lg \theta \tag{18}$$

Set

$$y = \lg F, x_0 = \lg \varepsilon, x_1 = \lg v_s, x_2 = \lg v_w, x_3 = \lg a_p, x_4 = \lg \theta$$

Then Eq. (19) can be converted to

$$y = x_0 + a \cdot x_1 + b \cdot x_2 + c \cdot x_3 + d \cdot x_4 \tag{19}$$

Based on the multiple linear regression equation, the transformed experimental data were regressed and analyzed to find the values of the coefficients in Eq. (19).

$$x_0, a, b, c, d$$

The value in Eq. (18) is then inverted. An empirical formula prediction model for grinding force in the form of a power exponent considering the fiber orientation angle can be derived. Based on the experimental results, the following empirical formula is established with the grinding force as the target:

The normal and tangential grinding force models for conventional grinding considering fiber orientation are as follows Eq. (20):

$$\begin{cases} F_n = 10^{-0.887} \cdot v_s^{-0.5634} \cdot v_w^{0.5966} \cdot a_p^{0.755} \cdot \theta^{0.00896} \\ F_t = 10^{-1.4772} \cdot v_s^{-0.5541} \cdot v_w^{0.6779} \cdot a_p^{0.8723} \cdot \theta^{0.0139} \end{cases} \tag{20}$$

The normal and tangential grinding force models for ultrasonically assisted grinding considering fiber orientation are as follows Eq. (21):

$$\begin{cases} F_n = 10^{-1.113} \cdot v_s^{-0.591} \cdot v_w^{0.6073} \cdot a_p^{0.8056} \cdot \theta^{0.0043} \\ F_t = 10^{-1.953} \cdot v_s^{-0.6095} \cdot v_w^{0.7892} \cdot a_p^{0.9547} \cdot \theta^{0.0466} \end{cases} \tag{21}$$

The empirical equations for the normal and tangential grinding force prediction models that combine ultrasonic amplitude and fiber orientation are in Eq. (22), respectively:

$$\begin{cases} F_n = 10^{-1.0418} \cdot v_s^{-0.5772} \cdot v_w^{0.602} \cdot a_p^{0.7083} \cdot \theta^{0.00664} \cdot A^{-0.0377} \\ F_t = 10^{-1.775} \cdot v_s^{-0.5818} \cdot v_w^{0.7336} \cdot a_p^{0.9135} \cdot \theta^{0.03025} \cdot A^{-0.0542} \end{cases} \tag{22}$$

3.3.3 Significance testing of empirical formula models

Significance tests were performed on the grinding force prediction model to determine the degree of model fit. Equations (4), (5), (6), (7), (11), (12), and (13) were analyzed for significance test, and the results of the statistical test are shown in Table 6. f represents the degrees of freedom of ANOVA, SS represents the sum of squares, MS represents the mean square value, and F represents the mean square ratio. U-F_n, and C-F_n represent the ultrasound-assisted normal grinding force and conventional normal grinding force, respectively. U-F_t, and C-F_t represent the ultrasound-assisted tangential grinding force and conventional tangential grinding force, respectively.

Table 6 demonstrates the significant test results of the grinding force models, and the p-value of each prediction model is less than 0.05. Therefore, the experimental grinding force prediction model is highly significant with a good state of fit and high confidence.

3.4 Range analysis and variance analysis of orthogonal test data

3.4.1 Range analysis results of different *fiber* orientation angles

Table 7 shows the range analysis results of the test results of 2.5D-C$_f$/SiC composites with fiber angles of 0°, 45°, and 90°, respectively. In the table, *K1*, *K2*, *K3*, and *K4*, respectively, represent the sum of the measured values of the grinding force index corresponding to levels 1, 2, 3, and 4 under each factor. *k1*, *k2*, *k3*, and *k4* respectively represent the average values of the measured values corresponding to levels 1, 2, 3, and 4 under each factor. *R* represents the range value of the influence of each factor on the grinding force results. OC stands for the optimal combination. *A*, *B*, and *C* represent line speed, feed speed, and grinding depth.

The results of the range analysis of 2.5D ultrasonically assisted grinding and conventional grinding orthogonal tests for 2.5D-C$_f$/SiC are shown in Table 7. The order of magnitude of the range values for different process parameters and fiber orientations is shown in Fig. 10. The results are as follows: When the fiber angle is 0°, the influence of process parameters on normal and tangential grinding forces of 2D ultrasound-assisted grinding in the experimental parameter range is in the same order of A > B > C, i.e., linear speed > feed speed > grinding depth. The process parameters affect the normal and tangential forces of conventional grinding in the same order, A > C > B, i.e., linear speed > grinding depth > feed rate. When the fiber orientation is 45°, the order of influence of process parameters on the normal grinding force of 2D ultrasonically assisted grinding is A > B > C, i.e., line speed > feed speed > grinding depth. The influence of process parameters on the ultrasonic tangential grinding force was in the order of A > C > B, i.e., line speed > grinding depth > feed speed. The different order of influence of process parameters on normal and tangential forces of 2D ultrasonically assisted grinding may be due to the effect of the 45° fiber orientation angle. The process parameters affect the normal and tangential forces of conventional grinding in the same order A > C > B, i.e., linear speed > grinding depth > feed rate. When the fiber orientation is taken as 90°, the influence of process parameters on the normal force and tangential force of 2D ultrasonic-assisted grinding is in the same order of A > C > B, i.e., line speed > grinding depth > feed speed. The influence of process parameters on normal force and tangential force of

Table 6 Analysis of significance test of regression equation of grinding force

	Source	F_n					F_t				
		f	SS	MS	F	P	f	SS	MS	F	P
0°-C	Regression	3	5.55294	1.85098	243.17	0	3	17.591	5.8638	13.1	0
	Error	12	0.09134	0.00761			12	5.37	0.4475		
	Summation	15	5.64428				15	22.961			
0°-U	Regression	3	6.0846	2.02819	54.83	0	3	11.2684	3.75614	66.44	0
	Error	12	0.4439	0.03699			12	0.6784	0.05653		
	Summation	15	6.5285				15	11.9468			
45°-C	Regression	3	5.95189	1.98396	280.48	0	3	6.6232	2.20772	212.34	0
	Error	12	0.08488	0.00707			12	0.1248	0.0104		
	Summation	15	6.03678				15	6.7479			
45°-U	Regression	3	6.5776	2.19253	120.89	0	3	7.3624	2.45414	118.29	0
	Error	12	0.2176	0.01814			12	0.249	0.02075		
	Summation	15	6.7952				15	7.6114			
90°-C	Regression	3	3.711	1.23699	79.32	0	3	4.3655	1.45518	98.38	0
	Error	12	0.1871	0.0156			12	0.1775	0.01479		
	Summation	15	3.8981				15	4.543			
90°-U	Regression	3	4.0963	1.36543	21.39	0	3	4.663	1.55435	28.77	0
	Error	12	0.7661	0.06384			12	0.6482	0.05402		
	Summation	15	4.8624				15	5.3113			
Integration of fiber angles-C	Regression	4	15.0103	3.75257	216.86	0	4	17.8845	4.47113	240.25	0
	Error	43	0.7441	0.0173			43	0.8002	0.01861		
	Summation	47	15.7544				47	18.6848			
Integration of fiber angles-U	Regression	4	16.4504	4.11261	96.45	0	4	22.7886	5.69716	88.74	0
	Error	43	1.8334	0.04264			43	2.7607	0.0642		
	Summation	47	18.2839				47	25.5493			
Integration of fiber angle and ultrasound	Regression	5	31.9253	6.3851	221.04	0	5	41.4182	8.2836	195.04	0
	Error	90	2.5997	0.0289			90	3.8224	0.0425		
	Summation	95	34.525				95	45.2406			

conventional grinding is in the same order, A > B > C, i.e. line speed > feed speed > grinding depth. As can be seen from Table 7, the optimal combinations of process parameters for normal and tangential grinding forces under 2D ultrasonically assisted grinding and conventional grinding conditions of 2.5D-C_f/SiC were the same for A1B1C1, i.e., a line speed of 23.60 m/s, a feed rate of 5 mm/min, and a depth of grind of 10 μm, when the fiber orientations were 0°, 45°, and 90°.

The machining parameters selected near and far from the optimal process parameter combinations for the two machining methods of TDUAG and CG for 2.5D-C_f/SiC composites are shown in Fig. 11a–d, respectively. The 3D contour plots selected in Fig. 11a and b are close to the optimal combination of process parameters. The linear speed is taken as 10.56 m/s, the feed rate is taken as 50 mm/min, and the grinding depth is taken as 10 μm. Figure 11a shows the 3D contour of TDUAG, the surface

roughness Sa is 0.236 μm, the normal force is 1.05 N, and the tangential force is 0.23 N. Figure 11b shows the 3D contour of CG, the surface roughness Sa is 0.259 μm, the normal force is 1.44 N, and the tangential force is 0.72 N. The three-dimensional profiles selected in Fig. 11c and d are away from the optimum combination of process parameters. The linear speed is taken as 0.66 m/s, the feed rate is taken as 100 mm/min, and the grinding depth is taken as 150 μm. Figure 11c shows the 3D contour of TDUAG, the surface roughness Sa is 0.66 μm, the normal force is 49.6 N, and the tangential force is 32.86 N. Figure 11d shows the 3D contour of CG. The surface roughness Sa was 0.82 μm, the normal force was 95.7 N, and the tangential force was 64.01 N. From Fig. 11, it can be seen that the TDUAG can significantly reduce the grinding force and surface roughness under the same processing conditions. The closer the processing parameters are to the optimal parameter combination, the better the processing effect is.

Table 7 Range analysis of grinding force for 0°, 45°, and 90° fiber orientation

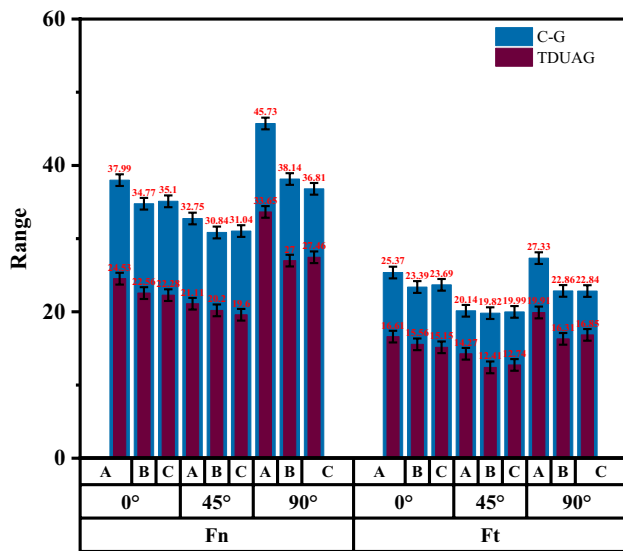|		$F_n(N)$ 0°			$F_n(N)$ 45°			$F_n(N)$ 90°			$F_t(N)$ 0°			$F_t(N)$ 45°			$F_t(N)$ 90°		
		A	B	C	A	B	C	A	B	C	A	B	C	A	B	C	A	B	C
K1	C	164.98	11.15	6.77	151.65	17.76	13.18	193.7	8.85	8.08	108.2	4.75	2.71	91.34	8.11	6.45	115.2	4.49	3.78
	U	108.99	8.32	4.55	101.28	12.98	7.52	141.8	6.16	5.86	70.08	1.42	0.88	64.41	7.11	4.63	84	2.5	2.69
K2	C	88.54	36.10	38.69	99.33	42.57	45.84	80.08	35.76	43.7	56.14	21.43	21.50	64.44	23.92	24.47	49.79	21.41	25.16
	U	79.88	31.27	34.05	84.32	33.25	42.15	67.24	28.2	35.66	49.77	16.03	17.06	51.85	17.26	20.41	40.53	16.96	19.94
K3	C	25.82	94.91	99.74	26.47	96.68	101.75	23.78	102.2	101.2	15.14	61.74	64.55	15.89	63.05	65.11	13.86	62.88	60.62
	U	20.63	82.26	88.13	17.51	79.93	85.9	20.33	87.97	79.3	10.76	53.15	54.81	9.84	52.33	52.81	11.45	53.18	47.66
K4	C	13.03	150.2	147.2	20.66	141.1	137.34	10.75	161.4	155.3	6.75	98.32	97.48	10.8	87.39	86.44	5.86	95.91	95.13
	U	10.88	98.54	93.66	16.83	93.78	84.37	7.17	114.2	115.7	3.65	63.65	61.5	7.35	56.75	55.6	4.38	67.72	70.07
k_1	C	41.25	2.79	1.69	37.91	4.44	3.30	48.41	2.21	2.02	27.05	1.19	0.68	22.84	2.03	1.61	28.79	1.12	0.95
	U	27.25	2.08	1.14	25.32	3.25	1.88	35.44	1.54	1.47	17.52	0.36	0.22	16.10	1.78	1.16	21	0.63	0.67
k_2	C	22.14	9.03	9.67	24.83	10.64	11.46	20.02	8.94	10.93	14.04	5.36	5.37	16.11	5.98	6.12	12.45	5.35	6.29
	U	19.97	7.82	8.51	21.08	8.31	10.54	16.81	7.05	8.92	12.44	4.01	4.27	12.96	4.32	5.10	10.13	4.24	4.99
k_3	C	6.46	23.73	24.94	6.62	24.17	25.44	5.95	25.56	25.29	3.79	15.44	16.14	3.97	15.76	16.28	3.47	15.72	15.16
	U	5.16	20.56	22.03	4.38	19.98	21.48	5.08	21.99	19.83	2.69	13.29	13.70	2.46	13.08	13.20	2.86	13.30	11.92
k_4	C	3.26	37.55	36.79	5.17	35.28	34.34	2.69	40.36	38.83	1.69	24.58	24.37	2.7	21.85	21.61	1.47	23.98	23.78
	U	2.72	24.64	23.42	4.21	23.45	21.09	1.79	28.54	28.92	0.91	15.91	15.38	1.84	14.19	13.9	1.10	16.93	17.52
R	C	37.99	34.77	35.1	32.75	30.84	31.04	45.73	38.14	36.81	25.37	23.39	23.69	20.14	19.82	19.99	27.33	22.86	22.84
	U	24.53	22.56	22.28	21.11	20.2	19.60	33.65	27.00	27.46	16.61	15.56	15.15	14.27	12.41	12.74	19.91	16.31	16.85
Order	C	ACB			ACB			ABC			ACB			ACB			ABC		
	U	ABC			ABC			ACB			ABC			ACB			ACB		
OC	C	A1B1C1			A1B1C1			A1B1C1			A1B1C1			A1B1C1			A1B1C1		
	U	A1B1C1			A1B1C1			A1B1C1			A1B1C1			A1B1C1			A1B1C1		

Fig. 10 Influence of three process parameters on the value of the extreme difference

3.4.2 Analysis of variance for different *fiber* orientation angles

Range analysis cannot distinguish data fluctuations caused by changes in test conditions (changes in factor levels) during a test from those caused by test errors nor can give a precise quantitative estimate of the significance of factor effects. Therefore, the results of the range analysis method are used as a reference only. A detailed analysis of the degree of influence (significance) of each parameter is also required to carry out an ANOVA on the orthogonal test data and, based on the results of the ANOVA to find the optimal combination of parameters, to achieve the optimization of the test parameters to achieve the processing effect of the minimum grinding force.

The F-test analyzes the data in Table 5 in ANOVA to determine the degree of influence of each factor on the test results, and the judgment criteria based on which the F-test is performed on the factors can generally be considered in four cases: (1) If $F >$ F0.01 (f_{factor}, f_e), then the factor has a highly significant effect on the test results and is recorded as **. (2) If F0.05 $(f_{factor}, f_e) < F <$ F0.01 (f_{factor}, f_e), then the factor has a significant effect on the test results, recorded as *. (3) If F0.10 $(f_{factor}, f_e) < F <$ F0.05 (f_{factor}, f_e), then the factor affects the test results and is recorded as (*). (4) If $F <$ F0.10 (f_{factor}, f_e), then the factor does not affect the test results. From the ANOVA results, we can see that the factor degrees of freedom $f_{factor} = 3$ and the error degrees of freedom $f_e = 6$. A check of the F-distribution table gives F0.01$(f_{factor}, f_e) =$ F0.01(3, 6) = 9.78, F0.05$(f_{factor}, f_e) =$ F0.05(3, 6) = 4.757, and F0.1$(f_{factor}, f_e) =$ F0.1(3, 6) = 3.29.

Table 8 shows the ANOVA results for each of the orthogonal test results in Table 5. Figure 12 visualizes the F-value results of the significance analysis F-test for the effect of each process parameter on the grinding force of 2.5D-C_f/SiC fibers oriented at 0°, 45°, and 90°. The results show that when the fiber angle is taken as 0°, the effects of the process parameters on the TDUAG force are linear speed, depth of grind, and feed in that order. This is inconsistent with the results of the range analysis. The range analysis does not take into account the effect of error, so the results of ANOVA prevail. The effects of process parameters on 2D ultrasonic tangential force were linear speed, feed rate, and grinding depth in that order. The effects of process parameters on normal and tangential forces for conventional grinding were in the same order, linear speed, grinding depth, and feed rate. This is consistent with the results of the range analysis in Table 7. When the fiber angle is taken as 45°, the effects of process parameters on the 2D ultrasonic normal grinding force are in the order of line speed, feed rate, and grinding depth. The effects on the ultrasonic tangential grinding force were line speed, grinding depth, and feed rate in that order. In conventional grinding, the effects of process parameters on normal and tangential forces were in the order of line speed, depth of grind, and feed rate. This is in agreement with the results of the range analysis in Table 7. When the fiber angle is taken as 90°, the effects of process parameters on the 2D ultrasonic normal and tangential forces are linear speed, feed rate, and depth of grind in that order. This is inconsistent with the results of the range analysis. The range analysis did not consider the effect of error and therefore was based on the results of the ANOVA. In contrast, the effects of normal and tangential grinding forces for conventional grinding were in the order of line speed, feed rate, and depth of grind. This is consistent with the results of the range analysis in Table 7.

ANOVA can more accurately perform error analysis, distinguishing the differences between experimental results caused by changes in factor levels from those caused by fluctuations in error. Therefore, it is more appropriate to take the ANOVA results for the optimal process parameters.

4 Conclusion

Single-factor experiments and orthogonal tests were conducted to investigate the two-dimensional ultrasound-assisted grinding versus conventional grinding for the grinding force pair of 2.5D-C_f/SiC. An empirical formula equation for the grinding force prediction model of 2.5D-C_f/SiC was developed by using power exponential function multiple linear regression analysis. Within the experimental parameters of this study, the following conclusions were drawn:
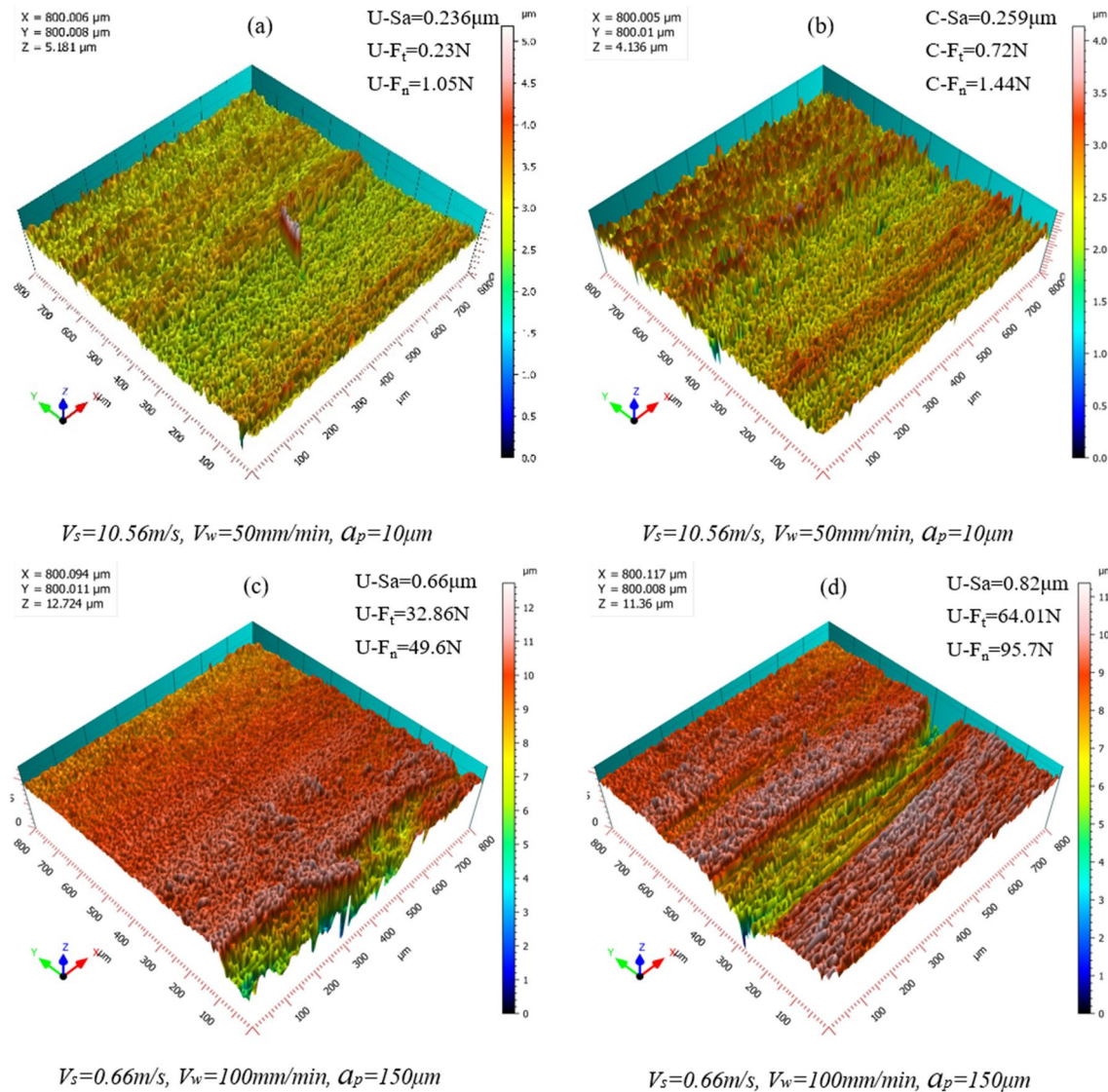
**Fig. 11** 2.5D-C/SiC three-dimensional contours of machined surfaces

(1) The grinding force varies negatively with linear velocity and positively with feed rate and depth of grind. 2D ultrasound reduces the grinding force, and the maximum reduction of the normal grinding force is 29.78% when the line speed is 10.48 m/s, the feed speed is 100 mm/min, the grinding depth is 50 μm, and along the 45° fiber direction. Under the same process conditions, the grinding force is the smallest along the 0° fiber orientation.

(2) Based on this experimental study, normal and tangential grinding force prediction models for 2.5D-C_f/SiC composites were developed for TDUAG and CG with three fiber orientations of 0°, 45°, and 90°, respectively. The grinding force prediction models for 2.5D-C_f/SiC composites for TDUAG and CG considering ultrasound amplitude, fiber orientation, and process parameters were developed, respectively.

(3) The order of significance of the influence of the grinding process parameters on the grinding force was determined. The order of influence of the process parameters on the ultrasonic normal force at 0° fiber orientation was linear speed, grinding depth, and feed rate. The order of influence of ultrasonic tangential force was line speed, feed rate, and depth of grind. For conventional grinding, the order of influence of process parameters on the normal force and tangential force was the same: line speed, depth of grind, and feed rate. When the fiber angle was 45°, the effects of the process parameters on the 2D ultrasonic normal force were in the order of line speed, feed rate, and grinding depth, while the effects on the ultrasonic tangential grinding force were in the order of line speed, grinding depth and feed rate. For conventional grinding, the effects of the process parameters

Table 8 Variance analysis of grinding force for 0°, 45°, and 0° fiber orientation

Source		F_n					F_t				
		f	SS	MS	F	P	f	SS	MS	F	P
0°-C	v_s	3	3631.2	1210.4	9.57	0.011	3	1616.2	538.72	9.34	0.011
	v_w	3	2907.1	969	7.66	0.018	3	1322.4	440.8	7.64	0.018
	a_p	3	2944.9	981.6	7.76	0.017	3	1366.9	455.65	7.9	0.017
	Error	6	759	126.5			6	346.2	57.7		
	Sum	15	10,242.1				15	4651.7			
0°-U	v_s	3	1665.5	555.165	200.45	0	3	752.66	250.886	301.87	0
	v_w	3	1345.36	448.454	161.92	0	3	657.3	219.099	263.63	0
	a_p	3	1394.2	464.732	167.8	0	3	643.04	214.348	257.91	0
	Error	6	16.62	2.77			6	4.99	0.831		
	Sum	15	4421.67				15	2057.99			
45°-C	v_s	3	2943.6	981.19	13.26	0.005	3	1135.2	378.4	17.8	0.002
	v_w	3	2291.6	763.87	10.32	0.009	3	981.6	327.2	15.39	0.003
	a_p	3	2318.2	772.75	10.44	0.009	3	1006.9	335.65	15.78	0.003
	Error	6	444.1	74.01			6	127.6	21.26		
	Sum	15	7997.5				15	3251.3			
45°-U	v_s	3	1465.99	488.66	45.28	0	3	633.92	211.308	51.83	0
	v_w	3	1091.03	363.68	33.7	0	3	463.81	154.602	37.92	0
	a_p	3	1059.22	353.07	32.72	0	3	466.51	155.503	38.14	0
	Error	6	64.75	10.79			6	24.46	4.077		
	Sum	15	3680.99				15	1588.7			
90°-C	v_s	3	5210	1736.5	8.14	0.015	3	1861.1	620.36	8.68	0.013
	v_w	3	3527	1175.7	5.51	0.037	3	1275.9	425.3	5.95	0.031
	a_p	3	3144	1048	4.91	0.047	3	1211.1	403.68	5.65	0.035
	Error	6	1280	213.3			6	428.7	71.45		
	Sum	15	13,161				15	4776.7			
90°-U	v_s	3	2774.7	924.9	13.62	0.004	3	980.9	326.98	14.17	0.004
	v_w	3	1905.9	635.3	9.36	0.011	3	695.7	231.9	10.05	0.009
	a_p	3	1748.3	582.77	8.58	0.014	3	665.2	221.74	9.61	0.01
	Error	6	407.4	67.9			6	138.5	23.08		
	Sum	15	6836.3				15	2480.3			
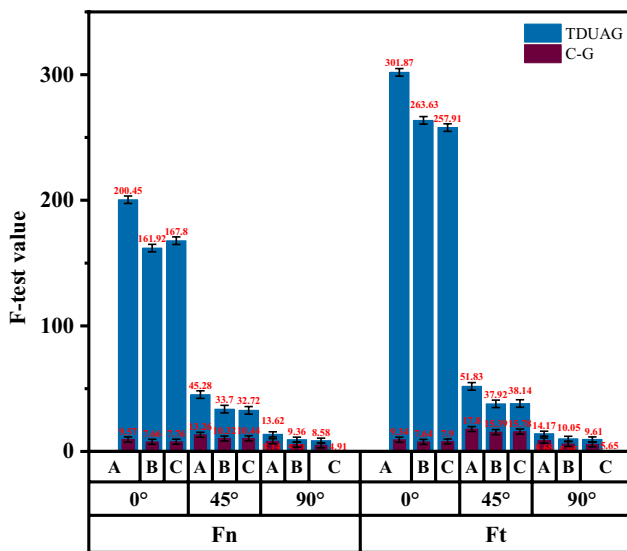
Fig. 12 Effect of three process parameters on ANOVA F-values

on the normal and tangential forces were in the order of linear speed, grinding depth, and feed rate. At a fiber angle of 90°, the effects of process parameters on the 2D ultrasonic normal and tangential forces were in the order of line speed, feed rate, and depth of grind, while the effects on the normal and tangential forces for conventional grinding were in the order of line speed, feed rate and depth of grind.

(4) The optimum combination of process parameters for this experiment was a linear speed of 23.60 m/s, a feed rate of 5 mm/min, and a grinding depth of 10 μm for grinding along the 0° fiber orientation.

Data Availability All data generated or analyzed during this study are included in this published paper.

Code availability Not applicable.

Declarations

Competing interests The authors declare no competing interests.

References

1. Xu QH, Xiao SL, Wang YQ et al (2024) Wear-induced variation of surface roughness in grinding 2.5D Cf/SiC composites [J]. Int J Mech Sci 264:108811
2. Zhao CW, Tu ZC, Mao JK et al (2023) The dynamic thermo-physical properties evolution and multi-scale heat transport mechanisms of 2.5D C/SiC composite under high-temperature air oxidation environment [J]. Composites Part B 263:110831
3. Xue R, Wang ZX, Zhang ZJ et al (2022) Anisotropic tribological behavior of LSI-based 2.5D needle-punched carbon fiber reinforced Cf/C–SiC composites [J]. Ceram Int 48:21283–21292
4. Zhai CT, Xu JK, Hou YG et al (2022) Effect of fiber orientation on surface characteristics of C/SiC composites by laser-assisted machining [J]. Ceram Int 45:6402–16413
5. Morel C, Baranger E, Lamon J et al (2024) The influence of the grinding process on the mechanical behavior of SiC/SiC composite tubes under uniaxial tension [J]. J Eur Ceram Soc 44(1):91–106
6. Diao QW, Zou HB, Ren XY et al (2023) A focused review on the tribological behavior of C/SiC composites: present status and prospects [J]. J Eur Ceram Soc 43:3875–3904
7. Diaz Oriol Gavalda, Luna Gonzalo Garcia, Liao Zhirong et al (2019) The new challenges of machining ceramic matrix composites (CMCs): review of surface integrity [J]. J Mach Tools Manuf 139:24–36
8. Du JG, Zhang HZ, Geng YM et al (2019) A review on machining of carbon fiber reinforced ceramic matrix composites [J]. Ceram Int 45:18155–18166
9. Li YC, Ge X, Wang H et al (2019) Study of material removal mechanisms in grinding of C/SiC composites via single-abrasive scratch tests[J]. Ceram Int 45(4):4729–4738
10. Hu Y, Ni DW, Chen BW et al (2024) Cf/(CrZrHfNbTa)C–SiC high-entropy ceramic matrix composites for potential multifunctional applications[J]. J Mater Sci Technol 182:132–140
11. Gavalda Diaz O, Axinte DA (2017) Towards understanding ceramic matrix composites' cutting and fracture mechanism [J]. International Journal of Machine Tools and Manufacture, 118–119 12–25
12. Yin JF, Xu JH, Ding WF et al (2021) Effects of grinding speed on the material removal mechanism in single grain grinding of SiCf/SiC ceramic matrix composite [J]. Ceram Int 47(9):12795–12802
13. Qin SQ, Zhu LD, Wiercigroch Marian et al (2022) Material removal and surface generation in longitudinal-torsional ultrasonic assisted milling [J]. Int J Mech Sci 227:107375
14. Yang ZC, Zhu LD, Zhang GX et al (2020) Review of ultrasonic vibration-assisted machining in advanced materials [J]. Int J Mach Tools Manuf 156:103594
15. Xie ZW, Liu ZQ, Wang B et al (2021) Longitudinal amplitude effect on material removal mechanism of ultrasonic vibration-assisted milling 2.5D-C/SiC composites [J]. Ceram Int 47:32144–32152
16. Wang JJ, Feng PF, Zang JF et al (2018) Experimental study on vibration stability in rotary ultrasonic machining of ceramic matrix composites: cutting force variation at hole entrance [J]. Ceram Int 44:14386–14392
17. Wang J, Zang JF, Feng PF et al (2017) Effects of tool vibration on fiber fracture in ultrasonic machining of C/SiC ceramic matrix composites[J]. Compos B 129:233–242
18. Zhou K, Xiao GJ, Huang Y et al (2024) Understanding machinability improvements and removal mechanism of ceramic matrix composites during laser-ablating assisted grinding [J]. Wear 538–539:205199
19. Zhou K, Xu JY, Xiao GJ et al (2019) Enhancing ductile removal of Cf/SiC composites during abrasive belt grinding using low-hardness rubber contact wheels[J]. Ceram Int 48(18):26042–26054
20. Zhou K, Xu JY, Xiao GJ et al (2022) A novel low-damage and low-abrasive wear processing method of Cf/SiC ceramic matrix composites: laser-induced ablation-assisted grinding [J]. J Mater Process Technol 302:117503
21. Chen J, An QL, Chen M et al (2020) Investigation on machined surface quality in ultrasonic-assisted grinding of Cf/SiC composites based on fracture mechanism of carbon fibers[J]. Int J Adv Manuf Technol 109(7):1583–1599
22. Chen J, Ming WW, An QL et al (2020) Mechanism and feasibility of ultrasonic-assisted milling to improve the machined surface quality of 2D Cf/SiC composites[J]. Ceram Int 46:15122–15136
23. Wang CG, Chen J, Zhang XX et al (2023) Effects of ultrasonic vibration assisted milling with laser ablation p retreatment on fatigue performance and machining efficiency of SiCf/SiC composites[J]. J Eur Ceram Soc 43(14):5925–5939
24. Dong ZG, Zhang HT, Kang RK et al (2022) Mechanical modeling of ultrasonic vibration helical grinding of SiCf/SiC composites [J]. Int J Mech Sci 234:107701
25. Ran YC, Kang RK, Dong ZG et al (2023) Ultrasonic assisted grinding force model considering anisotropy of SiCf/SiC composites[J]. Int J Mech Sci 250:108311
26. Sun GY, Zhao LL, Ma Z et al (2018) Force prediction model considering material removal mechanism for axial ultrasonic vibration-assisted peripheral grinding of Zerodur[J]. Int J Adv Manuf Technol 98:2775–2789
27. Xiong YF, Wang WH, Jiang RS et al (2022) Feasibility and tool performance of ultrasonic vibration-assisted milling-grinding SiCf/SiC ceramic matrix composite [J]. J Market Res 19:3018–3033
28. Xiao XZ, Zheng K, Liao WH et al (2016) Study on cutting force model in ultrasonic vibration assisted side grinding of zirconia ceramics[J]. Int J Mach Tools Manuf Design Res Appl 104:58–67
29. Lei XF, Xiang DH, Peng PC et al (2022) Establishment of dynamic grinding force model for ultrasonic-assisted single

abrasive high-speed grinding [J]. J Mater Process Technol 300:117420

30. Li W, Long CJ, Ma WQ et al (2023) Key technologies for laser-assisted precision grinding of 3D C/C-SiC composites[J]. J Eur Ceram Soc 43(10):4322–4335

31. Ren J, Hua D (2011) Grinding principle. [M]. Beijing, Publishing House of Electronics Industry,1 ,35–48

32. Wang Y, Li J (2024) Experimental study of the removal characteristics of C/SiC with different fiber structure arrangements for two-dimensional ultrasound-assisted grinding. [J]. Int J Adv Manuf Technol 131:3467–3485